CLS
COLLECTE LOCALISATION SATELLITES

Consortium Members

TU Delft Delft University of Technology | SATOC Satellite Oceanographic Consultants | DTU Space National Space Institute | isardSAT | National Oceanography Centre Natural Environment Research Council | NOVELTIS | Starlab Living Science | U.PORTO Faculdade de Ciências Universidade do Porto

ESA Cryosat Plus for Oceans

Product Validation Report (PVR) of the CPP SAR numerical retracker for oceans

Reference:	CLS-DOS-NT-13-156
Nomenclature:	CP4O-PVR-XXX
Issue:	1. 0
Date:	Jun. 24, 13

esa European Space Agency

cnes CENTRE NATIONAL D'ÉTUDES SPATIALES

Chronology Issues:			
Issue:	Date:	Reason for change:	Author
1.0	24/06/13	Creation of PVR Issue 1.0	T. Moreau F. Boy M. Raynal

People involved in this issue:		
Written by (*):	T. Moreau (CLS) F. Boy (CNES) M. Raynal (CLS)	Date + Initials:(visa or ref)
Checked by (*):	S. Labroue (CLS)	Date + Initial:(visa ou ref)
Approved by (*):	P. Thibaut (CLS)	Date + Initial:(visa ou ref)
Application authorized by (*):	XXX (ESA) N. Picot (CNES)	Date + Initial:(visa ou ref)

**In the opposite box: Last and First name of the person + company if different from CLS*

Index Sheet:	
Context:	
Keywords:	[Mots clés]
Hyperlink:	

Distribution:		
Company	Means of distribution	Names
CLS	Notification	

List of tables and figures

List of tables:

Aucune entrée de table d'illustration n'a été trouvée.

List of figures:

Applicable documents

Reference documents

RD 1 Manuel du processus Documentation
CLS-DOC

RD 2 Algorithm Theoretical Basis Document (ATBD) of the CPP SAR numerical retracker for oceans
S3A-NT-SRAL-00099-CNES

RD 3 Product Validation Report (PVR) of the CPP RDSAR processing for oceans
CLS-DOS-NT-13-155

Acronyms List

AIR	Azimuth Impulse Response
ATBD	Algorithm Theoretical Basis Document
BRF	Burst Repetition Frequency
CPP	Cryosat Processing Prototype
EO	Earth Observation
FSSR	Flat Sea Surface Response
LRM	Low Resolution Mode
LSE	Least Squares Estimator
NA	Not Applicable
NRT	Near Real Time
POD	Precise Orbit Determination
PTR	Point Target Response
PVR	Plan Validation Report
RD	Reference Document
RDSAR	Reduces Synthetic Aperture radar
RIR	Range Impulse Response
SAR	Synthetic Aperture radar
SIRAL	Synthetic Aperture Interferometric Radar Altimeter
SLA	Sea level Anomalies
SSB	Sea State Bias
SWH	Significant Wave Height

List of Contents

1. Introduction

1.1. Purpose and scope

This document is the Plan Validation Report (PVR) for the CryoSat-2 SAR L2 products over ocean, which is generated from the Cryosat Processing Prototype (CPP) by CNES. This document reports the validation results and error analyses of the CPP SAR L2 products, including direct comparisons with the reduced SAR measurements that provide a LRM reference over identical sea state.

1.2. Document structure

In the equatorial Pacific Ocean acquisition are performed in SAR mode. In this document we validate the CPP SAR derived SLA, SWH and Sigma-0 by cross-comparison with the validated CPP RDSAR over this region.

In Section 2 we describe the data used. In Section 3 the validation report of the CPP SAR L2 altimetric products is presented. In Section 4 we discuss our results and provide an outlook for future investigations.

2. Data and method overview

2.1. Selection of the test area

Since the CryoSat-2 acquisition mode mask has been changed on May 7th 2012 (see Figure 2.1), there is currently one large area operated in SAR mode, located in equatorial Pacific Ocean. This test area was selected by ESA among those proposed by an expert validation group, considering that the zone met the following criteria required:

1. low ocean variability (so easing the inter-mission calibration with conventional altimetry satellites like Jason 2 and in preparation to Sentinel-3),
2. few occurrences of rain and sigma0 blooms events (which could have different impacts on SAR and RDSAR),
3. mean SWH around 2 meters and mean wind around 7 meters (so the sea state is close to the mean conditions).

This site has been used for successfully validating the CPP reduced SAR data [RD 3]. Moreover, this area is of great interest for detecting ocean bathymetry features at high spatial resolution, in particular sea mounds mapping.

Its size is equal to 22° (latitude) x 75° (longitude) with longitudes ranging from 160°W to 85°W, and latitudes from 25°S to 3°S.

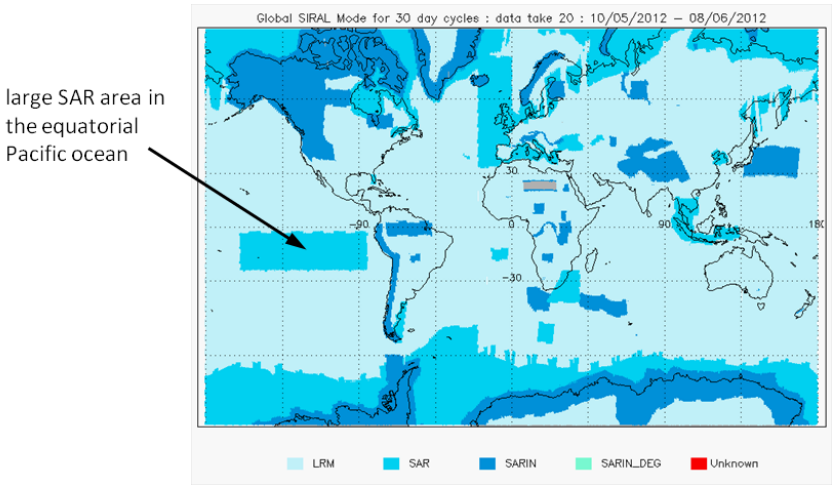

Figure 2.1: The mode mask, uploaded to CryoSat-2 in May 2012 (i.e. on May 7th).

2.2. Data used and method

2.2.1. Validation framework

Data in SAR mode are processed to produce both reduced SAR (also called pseudo-LRM) and SAR altimeter waveforms. Both are provided by the CPP chain processing according to the V13 RDSAR and SAR algorithms respectively (see related ATBD document). The RDSAR waveforms data are retracked using a conventional Brown ocean retracker [Amarouche et al., 2004] and the SAR waveforms by the CPP SAR numerical ocean retracker [Boy et al., 2012].

For this validation exercise that aims at measuring the quality of the results, different types of data analysis will be performed:

- we will use a small set of measurements taken along the track (subcycle 30, pass 82) spanning the period from 9:55 a.m. to 10:45 a.m. on May 7th 2012 (as shown in Figure 2.2). Only measurements located in the equatorial Pacific ocean SAR-mode area are selected, for latitude varying from -25° to -3°. The along track estimates from the collocated CPP RDSAR and SAR products will be examined through time series (mean and standard deviation on estimates will be presented).
- Secondly, we will use a whole 30-days subcycle of data from May 2012, but those data only that are located in the large test area. Retracked data using the CPP SAR method will be directly compared to the CPP RDSAR products through known metrics as standard deviations, biases, scatter plots and maps (of retracked data and of their differences). We will also identify possible dependencies between parameters.

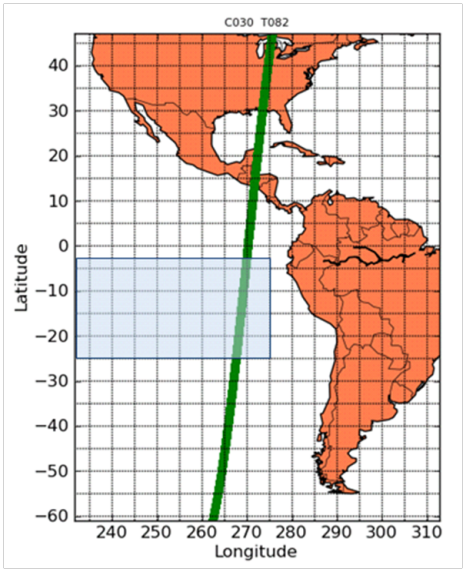

Figure 2.2: Segment of the track used (subcycle 30, pass 82).

2.2.2. Edited data

To analyze the consistency between RDSAR and SAR data in open ocean, only valid ocean data are selected. Specific editing criteria are applied:

- a valid flag is used, based on the validation task of CryoSat-2 performed by the CLS Space Oceanography Division. On-board retracked data are used for generating the flag in SAR-mode areas. With noise statistics and the shape of SAR altimeter waveforms so markedly different from those of the on-board LRM, the flag might be not adapted to edit SAR mode data.
- additional editing is applied to make sure to filter out all data points for which the SLA is higher than 1.5m above the reference level. This selection is more severe but ensure to eliminate all outliers (that may be related to some spurious observations caused by rain, blooms, or to some specifics events that can occur for instance after an orbit maneuver, or when an anomaly on an instrument impacts the quality of the measurement).

2.2.3. Correcting estimates through LUT

The Look-Up correction Table is used to correct the estimated parameters (range, significant wave height and sigma0) for errors resulting mainly from the Gaussian approximation of the Point Target Response (PTR) in the conventional Brown ocean retracker (others effects are also included in the correction LUT like the quantization of the signal, fast Fourier transform, speckle noise, etc.).

The CPP SAR method is based on the use of an amplitude numerical simulator that mimics the Cryosat-2 altimeter response in SAR mode (taking into account the real PTR and other characteristics of the altimeter without the need for approximations). This approach is considered to be more robust than analytical ones, particularly when faced with atypical observations (e.g., elliptical antenna pattern, off-nadir mispointing angles, real PTR) that are difficult to put into equations. There is thus no need of using a LUT in this case. Further work is though envisaged to evaluate the smallest errors in retracking parameters due to, for example, the speckle noise.

Only RDSAR range and SWH estimates have been corrected for errors caused by the analytical retracker approach (that uses an approximation of the PTR). We use the correction Lookup Table inherited from Jason-2 for this purpose. The range look-up correction could be assimilated to a bias lower than 2 cm, whereas the significant wave height look-up correction is as high as 20 cm and depend on waves (as displayed in Figure 2.3. We also know that the correction on the sigma0 is of the order of a few hundredths of a dB. It is neglected in regard to the overall error budget on this parameter.

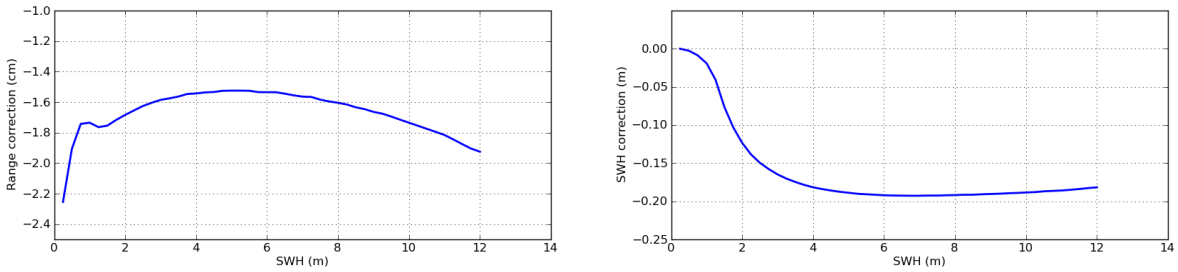

Figure 2.3: Range and SWH look-up table used for CPP products (corrections are in cm and m respectively).

An investigation is currently underway to update this correction LUT taking into account not only the approximation of the PTR in the retracking algorithm but also the characteristics of the CryoSat-2 altimeter (notably the ellipticity of the antenna) and the particular speckle reduction property of the RDSAR method (different from conventional altimetry mode).

2.2.4. Computing the sea level anomalies

Sea Level Anomalies (SLA) are computed by applying to the uncorrected sea level height the corrections available in the CPP products. The corrected sea level is defined as following for both datasets (RDSAR and SAR data):

$$SLA = Orbit - Range - i=0 NCi - MSS$$

where *Orbit* corresponds to the distance between the satellite and the ellipsoid, *Range* is the distance measured by the altimeter between the satellite and the sea surface, *MSS* is the Mean Sea Surface of the ocean over a long period and $i=0 NCi$ is the sum of all the corrections needed to take into account the atmospherically effects (wet and dry troposphere, ionosphere, inverse barometer) and the geophysical phenomena (ocean tides, high frequency atmospheric effects on ocean). The various dynamic auxiliary data that are needed to process these altimeter data are displayed in Table 1.

Note that the sea-surface bias (electromagnetic sea-surface bias) has not been considered in the corrections since no SSB solutions are available for both RDSAR and SAR methods at this stage. In this way the same corrections are applied for the RDSAR and SAR sea level measurements.

Orbit	Altitude of satellite above the reference ellipsoid - Cnes POE
Dry troposphere	Model dry tropospheric correction is computed at the altimeter time-tag from the interpolation of 2 meteorological fields that surround the altimeter time-tag. A dry tropospheric correction must be added (negative value) to the instrument range to correct this range measurement for dry tropospheric range delays of the radar pulse. From European Center for Medium Range Weather Forecasting
Wet troposphere	Model wet tropospheric correction is computed at the altimeter time-tag from the interpolation of 2 meteorological fields that surround the altimeter time-tag. A wet tropospheric correction must be added (negative value) to the instrument range to correct this range measurement for wet tropospheric range delays of the radar pulse. From European Center for Medium Range Weather Forecasting
Ionosphere	GIM ionospheric correction from NASA/JPL An ionospheric correction must be added (negative value) to the instrument range to correct this range measurement for ionospheric range delays of the radar pulse.
Ocean tide and loading tide	Geocentric ocean tide height (solution 1): GOT4.8 from GSFC Includes the loading tide and equilibrium long-period ocean tide height. The permanent tide (zero frequency) is not included in this parameter because it is included in the geoid and mean sea surface.
Solid Earth tide	Solid earth tide height is calculated using Cartwright and Taylor tables and consisting of the second and third degree constituents. The permanent tide (zero frequency) is not included. From Cartwright and Edden [1973] Corrected tables of tidal harmonics - J. Geophys. J. R. Astr. Soc., 33, 253-264.
Pole tide	Computed from Wahr [1985] Deformation of the Earth induced by polar motion - J. Geophys. Res. (Solid Earth), 90, 9363-9368.
Combined atmospheric correction	Also known as high frequency fluctuations of the sea surface topography which contains the combined atmospheric corrections (from MOG2D model + inverse barometer)
Mean Sea Surface	MSS_CNES_CLS-2011: mean sea surface height above reference ellipsoid from CLS/CNES

Table 1: Products corrections overview.

2.2.5. Computing the off-nadir from star stracker

The numerical CPP SAR retracking is based currently on a 3-parameters model (range, significant wave height, amplitude) that accounts for varying off-nadir mispointing angles in both axes (along-track and cross-track directions). Those angles, T_{across} and T_{along}, are obtained from the star tracker information, roll and pitch angles, T_{roll} and T_{pitch}, and pre-computed angular biases (a,b) corresponding to the angular alignment between the star tracker boresight and the altimeter electromagnetic axis. T_{across} and T_{along} are given by:

$$Tacross=Troll+a$$

$$Talong=Tpitch+b$$

To find the roll and pitch biases we use an iterative least-square estimation algorithm that consists in minimizing the errors between the mispointing angles $\xi 2$ estimated from LRM data and the mispointing angles, $Tacross2+Talong2$, obtained from star tracker [RD 2]. A comparison between those two quantities will be performed over the SAR mode test area to ensure consistent quality of the mispointing data injected as input parameter to the numerical SAR retracker.

3. Validation results and overall assessment

The overall objective of this validation exercise is to ensure that the CPP SAR processing algorithm allows to obtain the precision and resolution SAR-mode capabilities as they are theoretically expected, but also that the accuracy and reliability of the retrieved geophysical parameters are consistent with the LRM data.

In the following, the validation of the CPP SAR algorithm (as described in the ATBD document [RD 2]) is performed with:

- the collocated CPP RDSAR data (that have been validated and reported in the PVR [RD 3]). Direct comparisons of the SLA, SWH, Sigma-0 derived from RDSAR and SAR are performed within the test area. In addition, roll and pitch-mispointing angles obtained from biased star tracker information (and used as input of the SAR estimation processing) are compared to the mispointing angles derived from the ocean retracker to analyze their consistency.
- the current CPP CryoSat-2 LRM (that is routinely assimilated in the DUACS multimission altimeter products). Comparisons of the SLA, SWH, Sigma-0, mispointing estimates in a SAR/LRM mode transition region, are performed.

3.1. Along track SAR and RDSAR products

Figure 3.1 shows the 1 Hz CPP RDSAR and SAR products plotted along the track (pass 82 of subcycle 30), in the restricted equatorial Pacific test area (as the pass is descending, this figure has to be read from right to left following decreasing latitudes).

In these plots, we can see that the SLA/SWH RDSAR and SAR are in a quite good agreement with, to note, however, a slight bias that will be determined in our further analyses using one subcycle of data. RDSAR and SAR backscatter coefficients (Sigma0) are seemingly biased too (as a first tentative, only rough calibration has been performed leading to an imprecise shift to both parameters with respect to the Jason-2 mission reference). The most relevant result is their apparent similarity to capture same ocean structures that highlights the ability of the CPP SAR method to retrieve very consistent sigma0. On the other hand, these figures show a comparison of the square of the off-nadir angle obtained with the star tracker and the 4-parameters Brown ocean

retracker. The first processed at 0.1 Hz is obviously less noisy than the 1 Hz RDSAR retrieved mispointing angle. They are however in a good agreement.

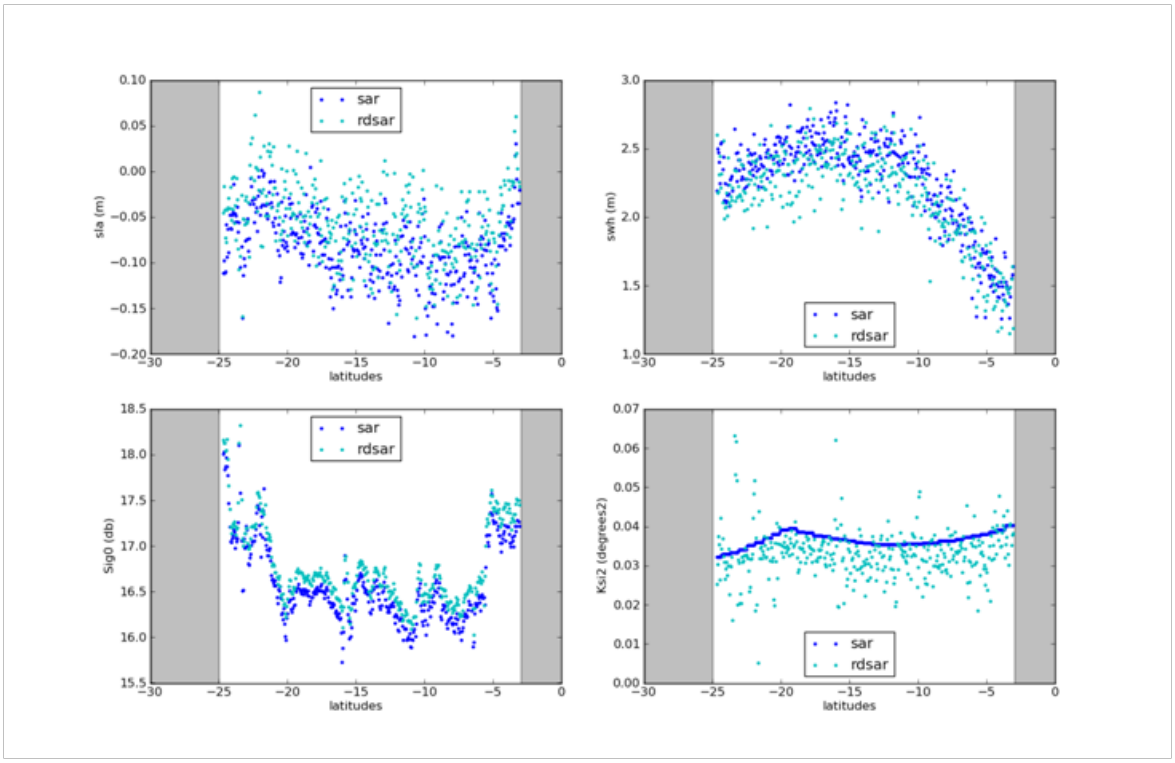

Figure 3.1: Sea Level Anomalies (upper left), significant wave height (upper right), Sigma0 coefficient (lower left) and mispointing angle (lower right) at 1 Hz from RDSAR and SAR altimeter data - subcycle 30 - pass 82.

Figure 3.2 gives the corresponding 1 Hz noises on the SLA/SWH parameters for the CryoSat-2 pass 82 of the subcycle 30. As expected the SAR parameter data are less noisy than the RDSAR parameter data.

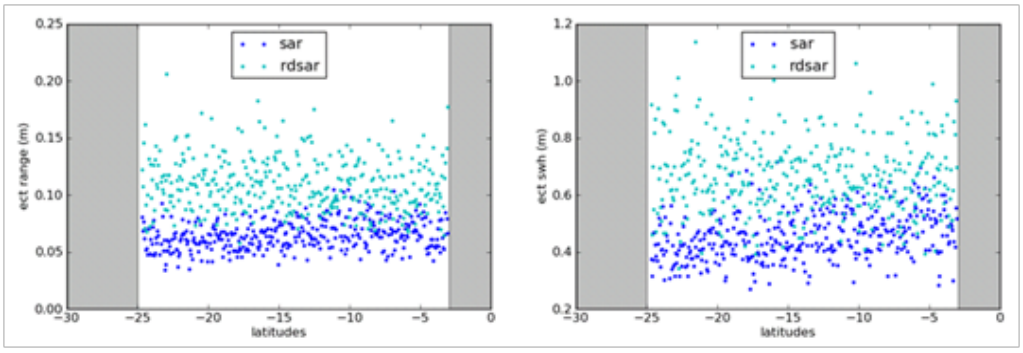

Figure 3.2: Precision of range (left), SWH (right) for along track RDSAR and SAR altimeter data.

The next section shows a validation of these results based on a larger amount of data (up to one subcycle of data).

3.2. SAR altimeter products evaluation based on several passes of data

Figure 3.3 shows the performance curves of 1 Hz range (1 Hz range standard deviation vs. SWH) and 1 Hz SWH (1 Hz SWH standard deviation vs. SWH) for RDSAR and SAR processing based on several passes (subcycle 30) of data acquired over the equatorial Pacific SAR mode region. For SWH of 2 m the precision of 1 Hz range is 10.4 cm in RDSAR and 5.6 cm in SAR. Similarly, the precision of 1 Hz SWH is 64 cm in RDSAR and 41 cm in SAR.

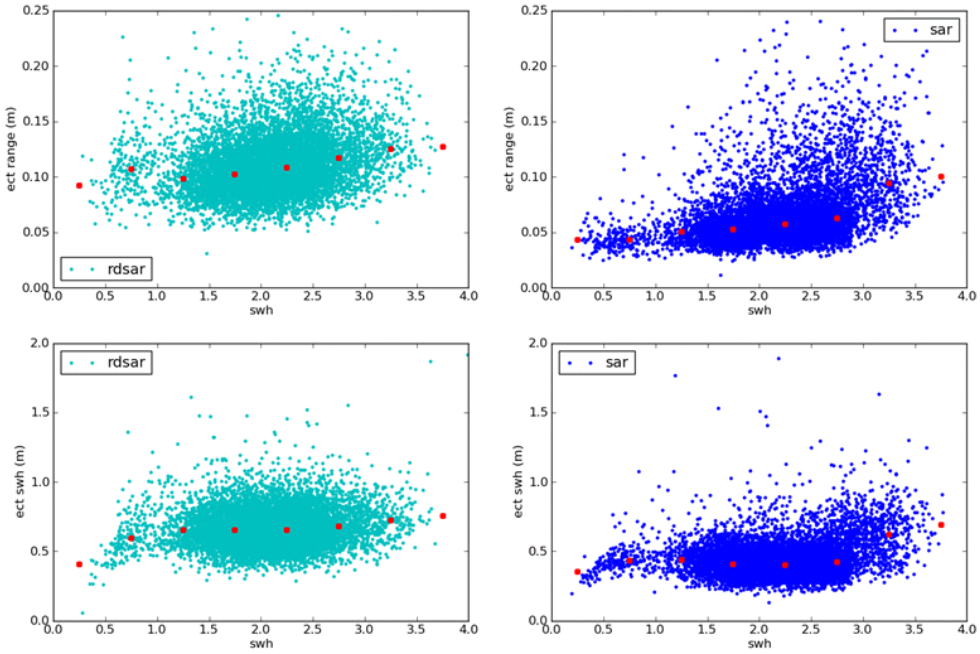

Figure 3.3: Precision of SLA (top) and SWH (bottom) from open sea RDSAR (left) and SAR (right).

The Figure 3.4 displays the scatter plot of the CPP RDSAR versus SAR data (SLA, SWH, sigma0 coefficient and mispointing angle) for several passes of subcycle 30. The linear regression shows a very good agreement between the two processing for SLA, SWH and sigma0 data over the region (for SLA: slope 0.92, for SWH: slope 1.07, and for sigma0: 0.98). For the mispointing angles, the 1 Hz RDSAR estimates is significantly noisier than the duplicated 0.1 Hz start tracker information. It makes the comparison between the two parameters a bit meaningless, in particular with a small set of data (about ten of tracks).

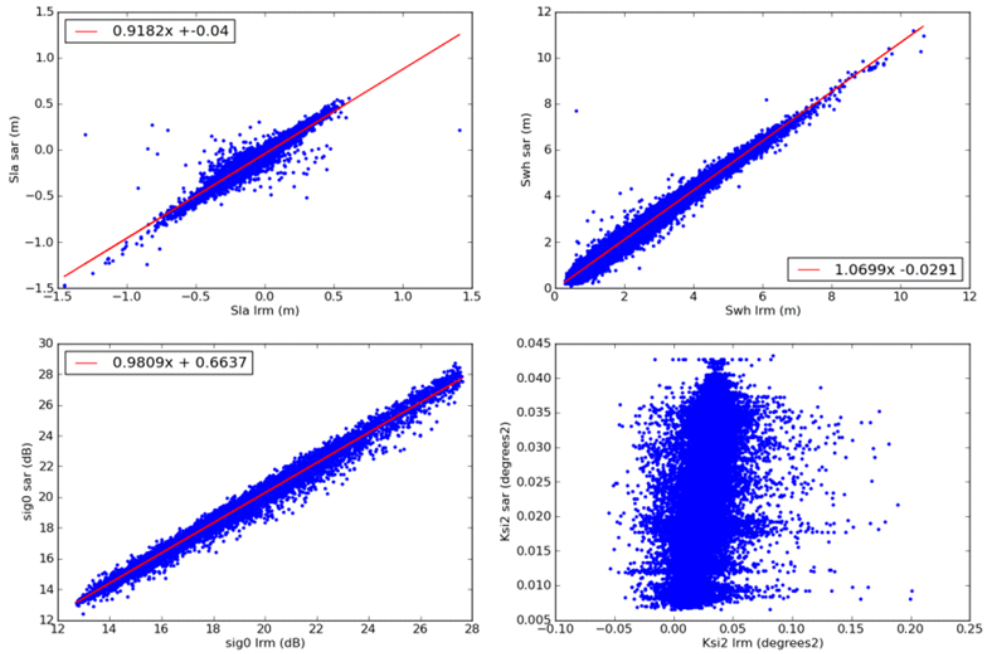

Figure 3.4: Scatterplot of SLA (upper left), SWH (upper right), Sigma0 coefficient (lower left) and mispointing angle (lower right) from open sea RDSAR and SAR data.

3.3. Analysis bench of one subcycle of data

This section shows some results of the CLS analysis bench, which is dedicated to routinely compare RDSAR and SAR products through several statistical parameters such as mean, standard deviation, maps and dependencies. Validation results are presented for both ascending and descending passes from the subcycle 30 (on May 2012).

3.3.1. Histogram of parameters

The comparison between the RDSAR and SAR altimeter products underlines a global bias of near 10 cm in waves (see Figure 3.5) and 3 cm in range (see Figure 3.6 and Figure 3.7), in the equatorial Pacific test area.

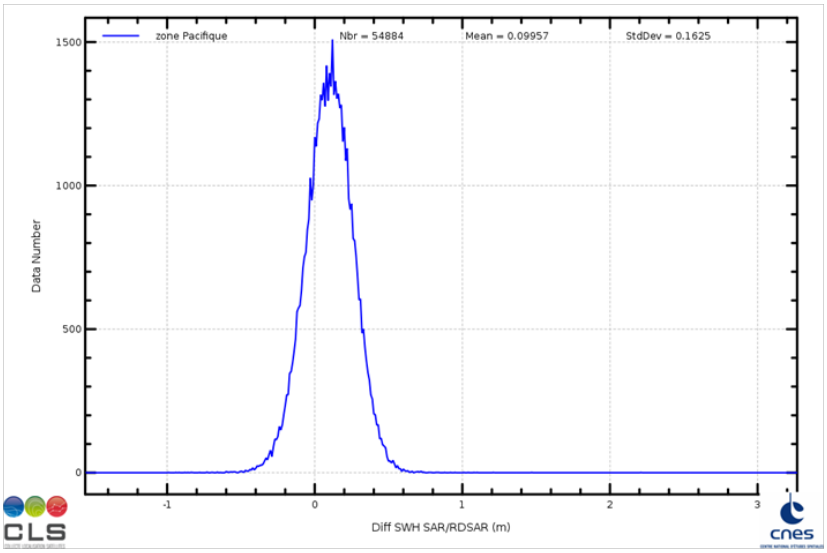

Figure 3.5: Histogram of difference of SWH from open ocean SAR and RDSAR data - subcycle 30.

3.3.1.1. Ascending tracks

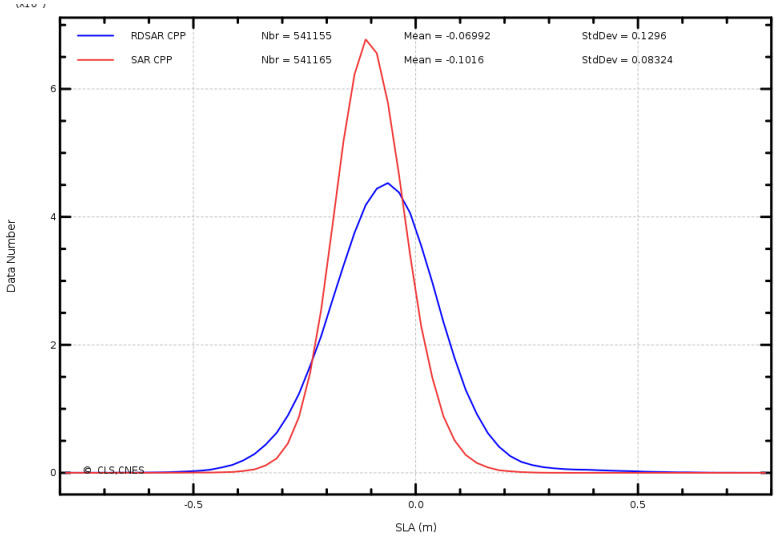

Figure 3.6: Histogram of SLA for the RDSAR and SAR - subcycle 30 (ascending tracks).

3.3.1.2. Descending tracks

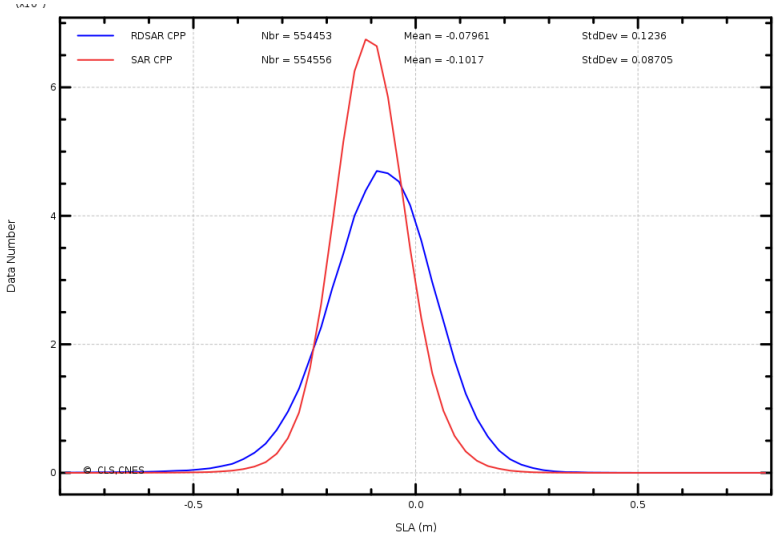

Figure 3.7: Histogram of SLA for the RDSAR and SAR - subcycle 30 (descending tracks).

3.3.2. Cartography of parameter

The along track 20 Hz measurements are used to construct a mean map (averaged values in each 2°x2° grid box) of the RDSAR and SAR estimates, but also their differences and others parameters (in particular the radial velocity and the across-track mispointing angle that may impact the retrievals). In this way, we can easily observe the geographical distribution of those parameters and the mapping biases between SAR and RDSAR products.

The Figure 3.8 and Figure 3.9 represent the mean maps of those data over the equatorial Pacific test area for the subcycle 30 (during May 2012). We can see that the spatial pattern of the differences between RDSAR and SAR data is not constant in ascending and descending tracks. They appear mostly correlated to the variation of the orbits (given by the radial velocity), which show a strong temporal variability that is correlated with the variability of the wave heights during the subcycle (CryoSat-2 mission is not optimised for ocean observation in real time since the subcycle needs 30-days for sampling the whole ocean). As a consequence, the geographical distribution of the differences between the RDSAR and SAR products also vary with waves. An illustration of the variations is given on Figure 3.8 where the SLA bias spread from -1 cm to +1 cm around its mean value, corresponding to wave heights, from 1.5 m to 3 m. A dependency analysis in next sections will help to identify the possible dependencies of the SLA data on across-track mispointing angle, significant wave height, or radial velocity without the temporal variability effect.

3.3.2.1. Ascending tracks

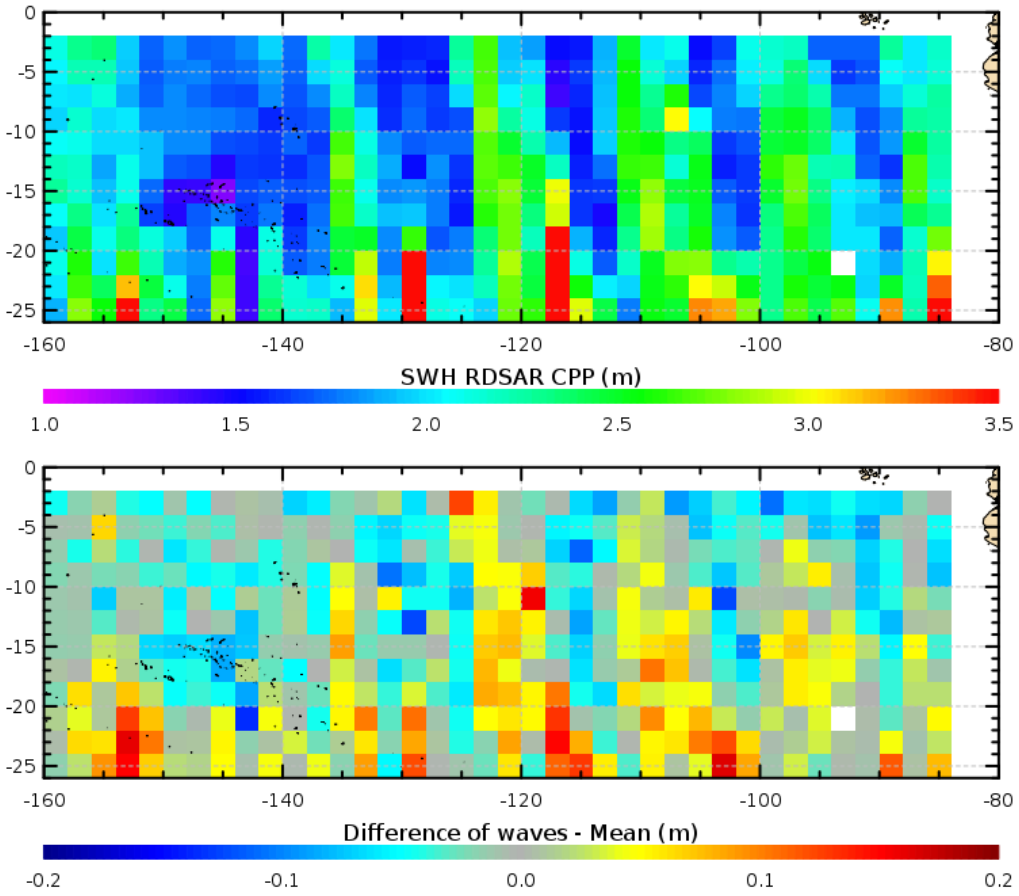

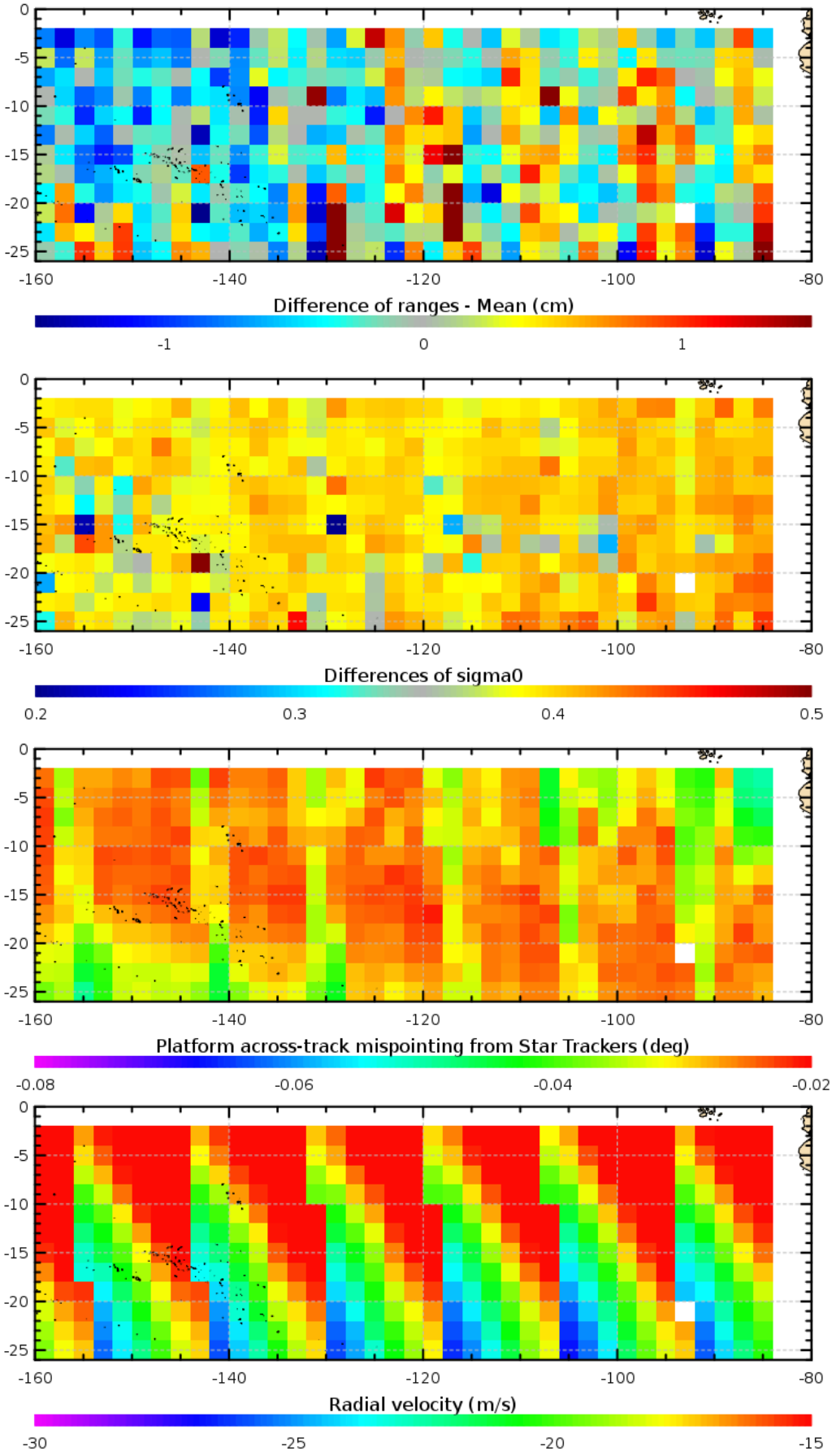
0
-5
-10
-15
-20
-25
-160
-140
-120
-100
-80
Difference of ranges - Mean (cm)
-1
0
1
Differences of sigma0
0.2
0.3
0.4
0.5
Platform across-track mispointing from Star Trackers (deg)
-0.08
-0.06
-0.04
-0.02
Radial velocity (m/s)
-30
-25
-20
-15

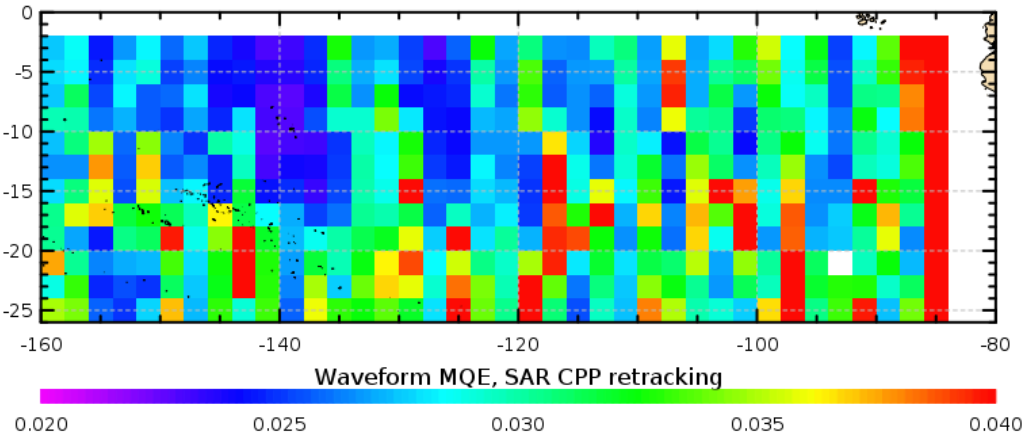

Figure 3.8: From top to bottom: (first row) Mean of SWH RDSAR; (second row) mean of the SWH difference between SAR and RDSAR; (third row) mean of the SLA difference between SAR and RDSAR; (fourth row) mean of the sigma0 difference between SAR and RDSAR; (fifth row) mean of the across-track mispointing angle obtained from star tracker information; (sixth row); mean of the radial velocity; (seventh row) mean of the MQE of the SAR altimeter retracking.

3.3.2.2. Descending tracks

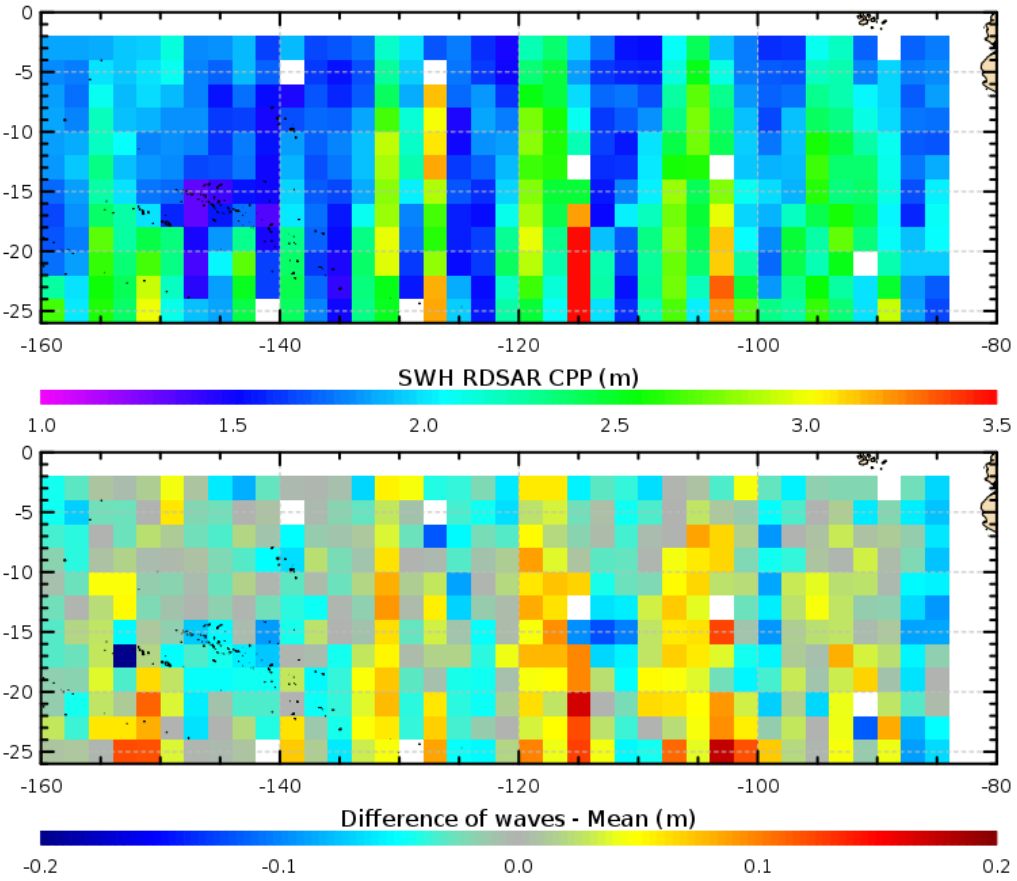

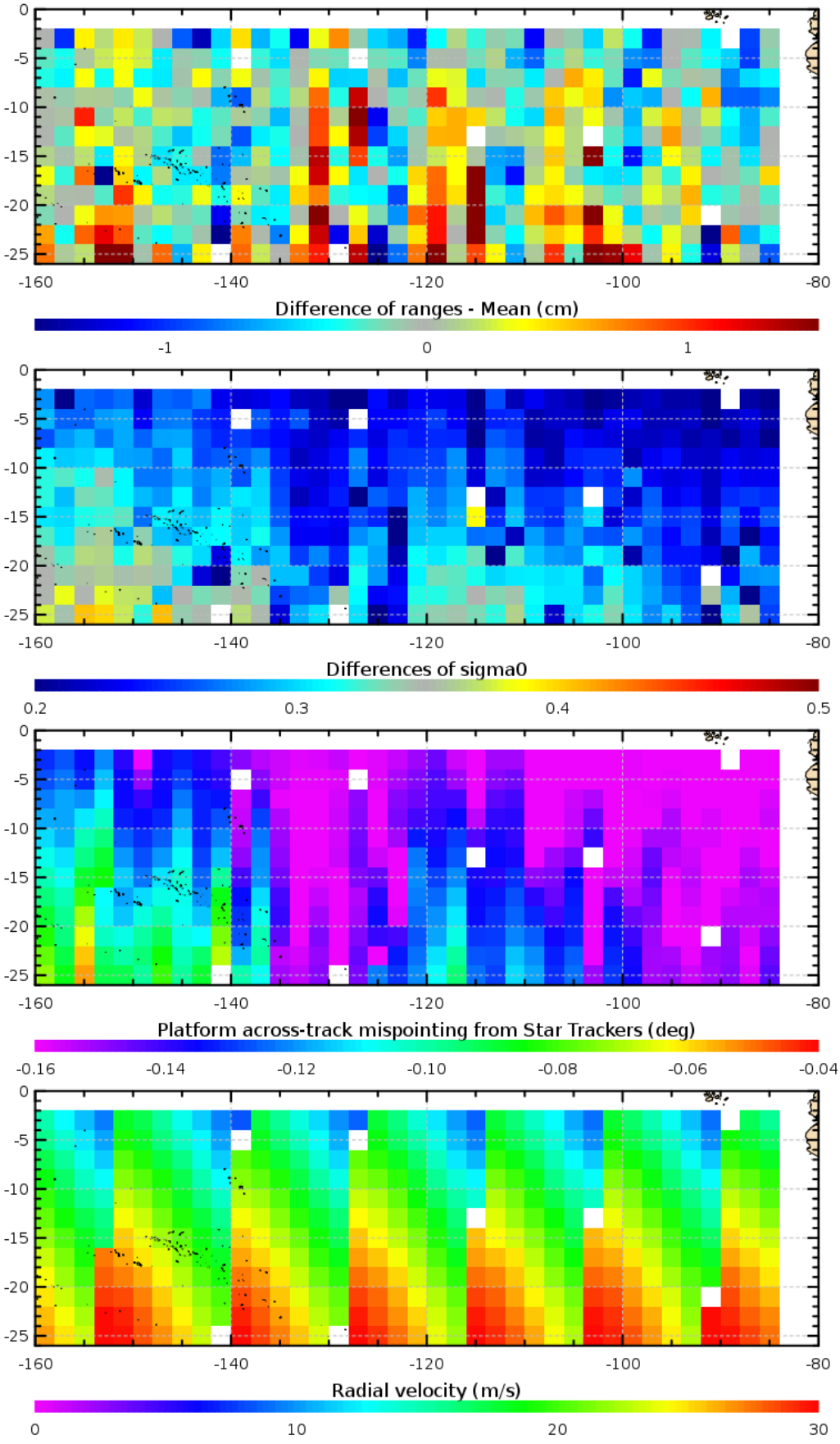
0
-5
-10
-15
-20
-25
-160
-140
-120
-100
-80
Difference of ranges - Mean (cm)
-1
0
1
Differences of sigma0
0.2
0.3
0.4
0.5
Platform across-track mispointing from Star Trackers (deg)
-0.16
-0.14
-0.12
-0.10
-0.08
-0.06
-0.04
Radial velocity (m/s)
0
10
20
30

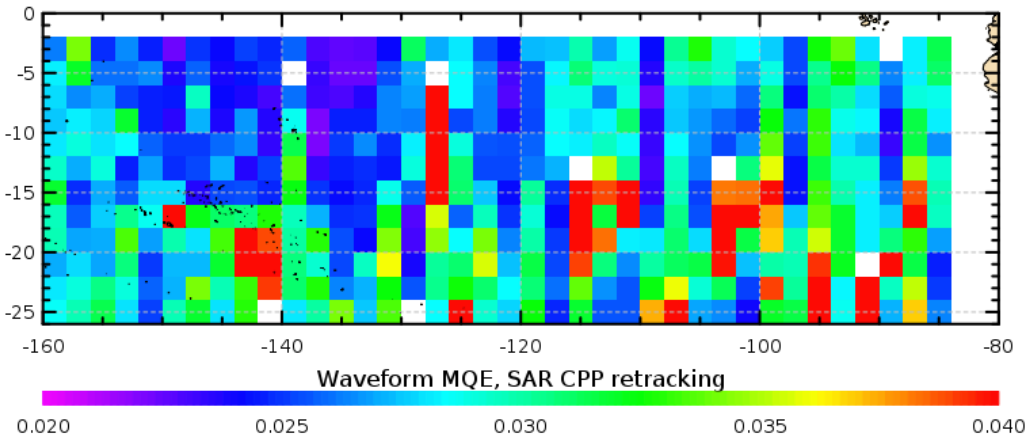

Figure 3.9: From top to bottom: (first row) Mean of SWH RDSAR; (second row) mean of the SWH difference between SAR and RDSAR; (third row) mean of the SLA difference between SAR and RDSAR; (fourth row) mean of the sigma0 difference between SAR and RDSAR; (fifth row) mean of the across-track mispointing angle obtained from star tracker information; (sixth row); mean of the radial velocity; (seventh row) mean of the MQE of the SAR altimeter retracking.

3.3.3. Dependencies between parameters

Let's now analyse the sensitivity of the retrievals to the across-track mispointing angle and the radial velocity.

In Figure 3.10 and Figure 3.12, the difference of ranges between SAR and RDSAR data is plotted versus SWH and the across-track mispointing angle obtained from the star tracker information. The Figure 3.11 and Figure 3.13 plot the same parameter as a function of SWH and the radial velocity. Both are displayed with the associated number of measurements taken into account per box (box width for SWH: 10 cm, for across-track mispointing angle: 0.004° and for the radial velocity: 1.4 ms^{-1}). Those results show no apparent dependencies of the numerical SAR model with respect to the across mispointing angle and the radial velocity. This was already confirmed through studies funded by CNES [Labroue et al., 2013] and based on a larger amount of CPP data (the whole SAR mode areas and several subcycle of data). They have also concluded to very negligible dependencies.

These figures also show the ranges dependency on SWH over the region. The RDSAR and SAR ranges are here corrected for all usual corrections except for the sea state bias that is not available for both processing. From these figures, we can estimate the dependency between the range difference and SWH. It appears to be equal to +0.5% SWH. Because the applied LUT correction for the RDSAR range does not exhibit any SWH dependency, this 0.5% SWH may then correspond to the additional SAR sea state bias with respect to the RDSAR one.

3.3.3.1. Ascending tracks

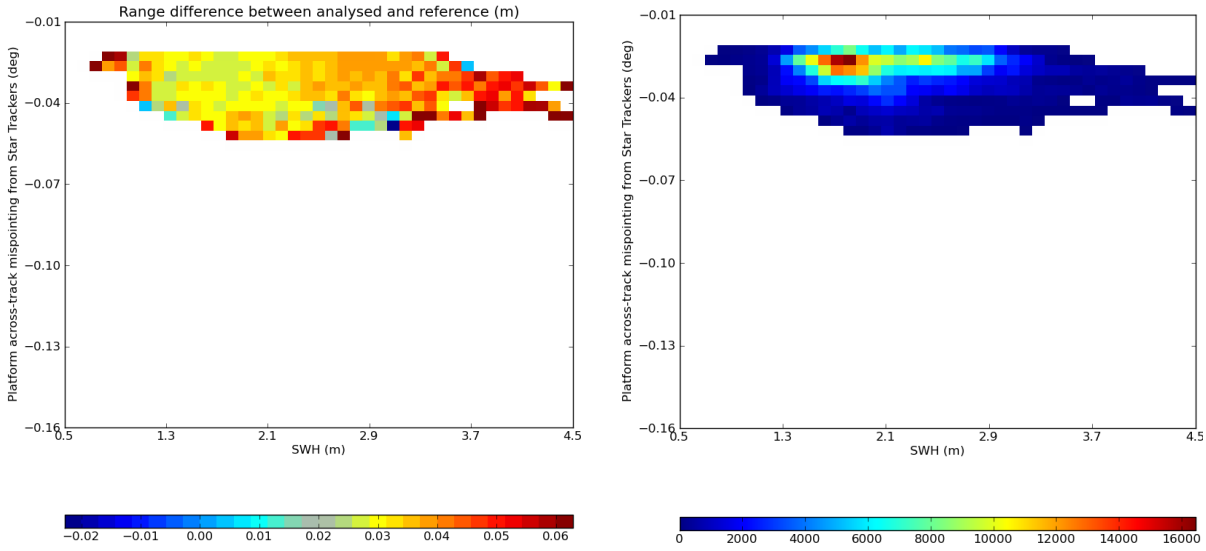

Figure 3.10: (left) Dependencies of the differences of the SLA data (SAR - RDSAR) with SWH and the across-track mispointing angle for the subcycle 30. (right) Density of points.

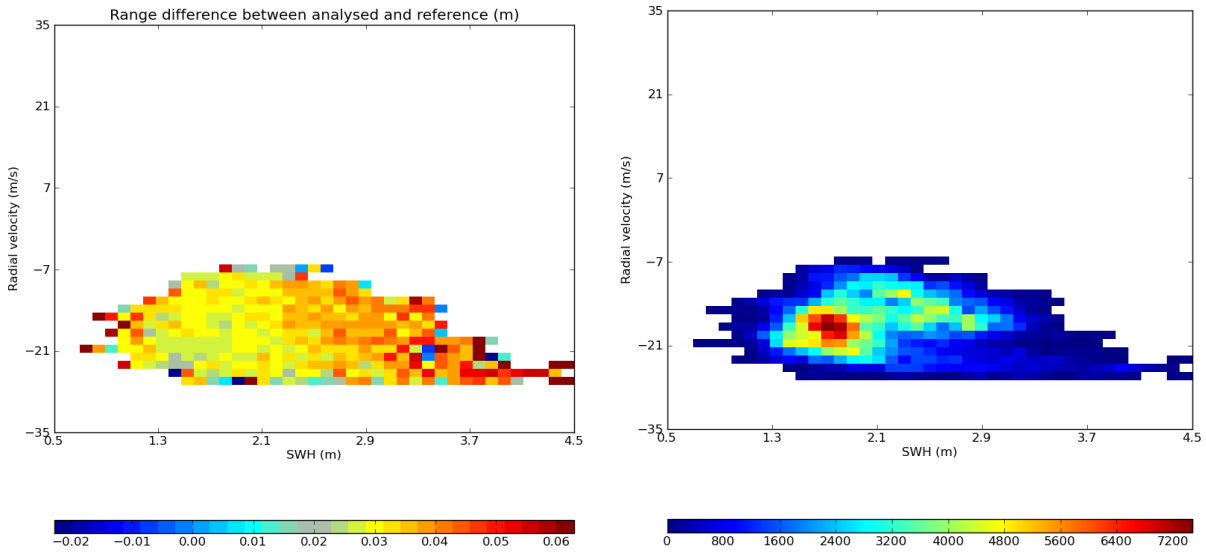

Figure 3.11: (left) Dependencies of the differences of the SLA data (SAR - RDSAR) with SWH and the radial velocity for the subcycle 30. (right) Density of points.

3.3.3.2. Descending tracks

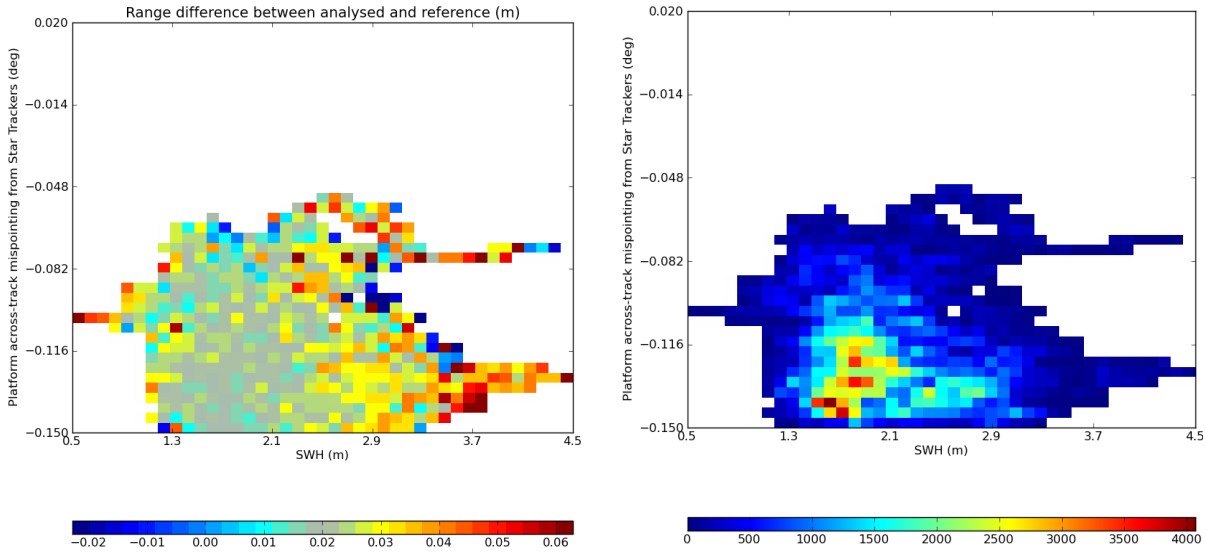

Figure 3.12: (left) Dependencies of the differences of the SLA data (SAR - RDSAR) with SWH and the across-track mispointing angle for the subcycle 30. (right) Density of points.

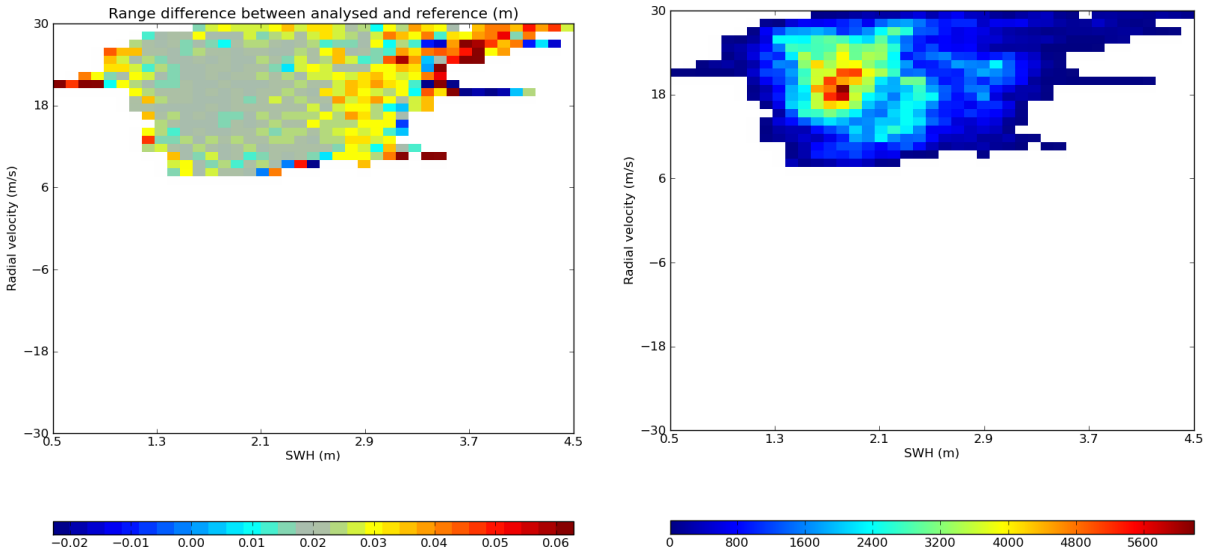

Figure 3.13: (left) Dependencies of the differences of the SLA data (SAR - RDSAR) with SWH and the radial velocity for the subcycle 30. (right) Density of points.

3.3.4. Spectral analysis of parameters

Besides the potential benefit of the SAR mode data in term of noise precision and ground resolution, the SAR altimeter data offer notably the ability to measure the content of the oceanic signal at high wavelength (mesoscale) where LRM mode is affected by correlated errors (seen as a spectral hump on the Figure 3.14 and Figure 3.15). The Figure 3.14 and Figure 3.15 show the energy spectrum of the SLA for the CPP RDSAR and SAR processing over the equatorial Pacific SAR region. We can see that the SAR SLA spectrum (red curve) perfectly follows the slope of the oceanic signal up to 50 km whereas the reduced SAR SLA spectrum (blue curve) breaks off the signal at 100 km.

Finally the SAR altimetry allows 1 Hz product users to recover smaller wavelengths (10-80 km) of interest for oceanography, where conventional altimeter mode needs to use complex waveform processing, dedicated retrackers or post-processing (e.g. Singular Value Decomposition algorithm) to edit out spurious data from historical LRM datasets and reduce both the noise level and the spectral hump. In addition the SAR data provide a noise level close to 5.5 cm at 20 Hz (the full altimetry resolution) whereas the precision of LRM altimeters is equal to 8-9 cm (and 11 cm with the CPP RDSAR method).

3.3.4.1. Ascending tracks

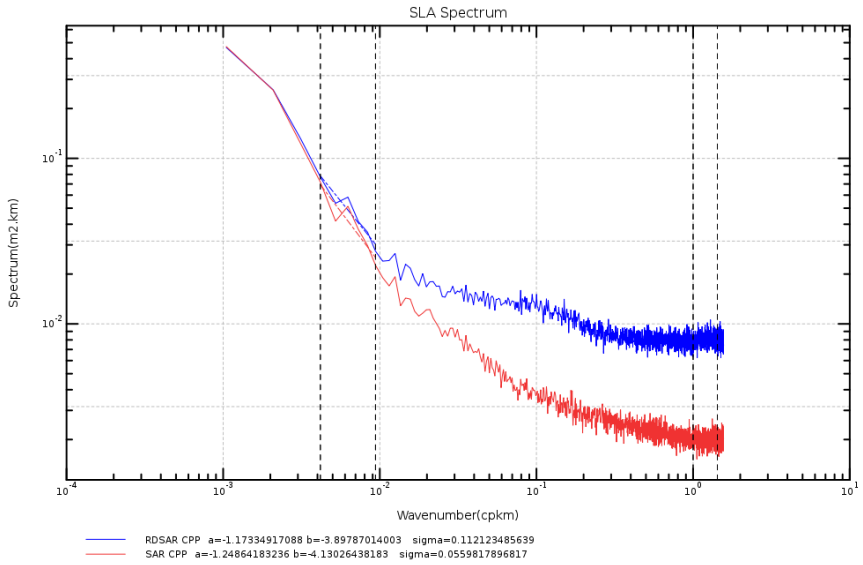

Figure 3.14: The mean sea level anomalies spectrum from RDSAR (blue) and SAR (red).

3.3.4.2. Descending tracks

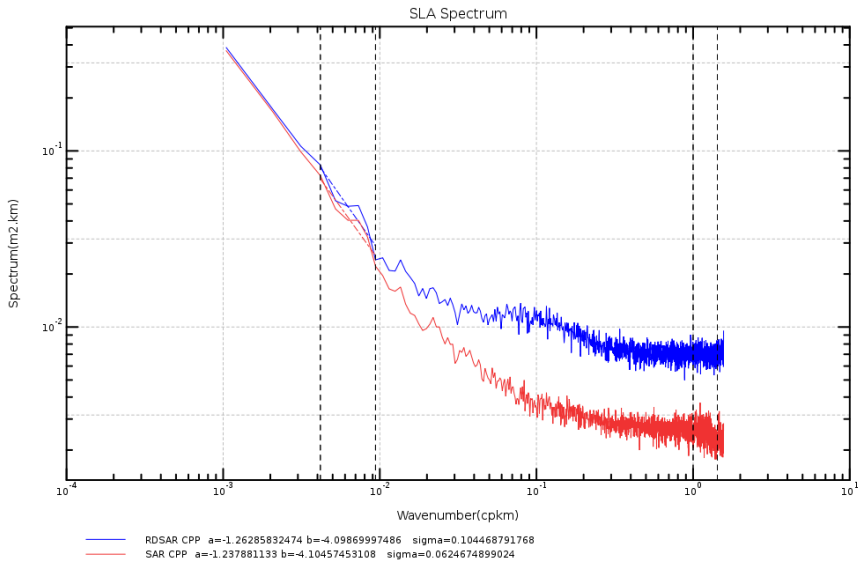

Figure 3.15: The mean sea level anomalies spectrum from RDSAR (blue) and SAR (red).

3.4. Assessment of the SAR/LRM data continuity

3.4.1. Map of estimates

Maps of LRM and SAR products in the equatorial Pacific test area are plotted in Figure 3.16. They are calculated globally (without separating ascending and descending passes). We can see a very good general agreement between LRM and SAR data over the region and notably at the transition between modes. SAR retrieval results are found to be very consistent with the ocean structure as observed by the LRM. Slight differences in mispointing angle are however present.

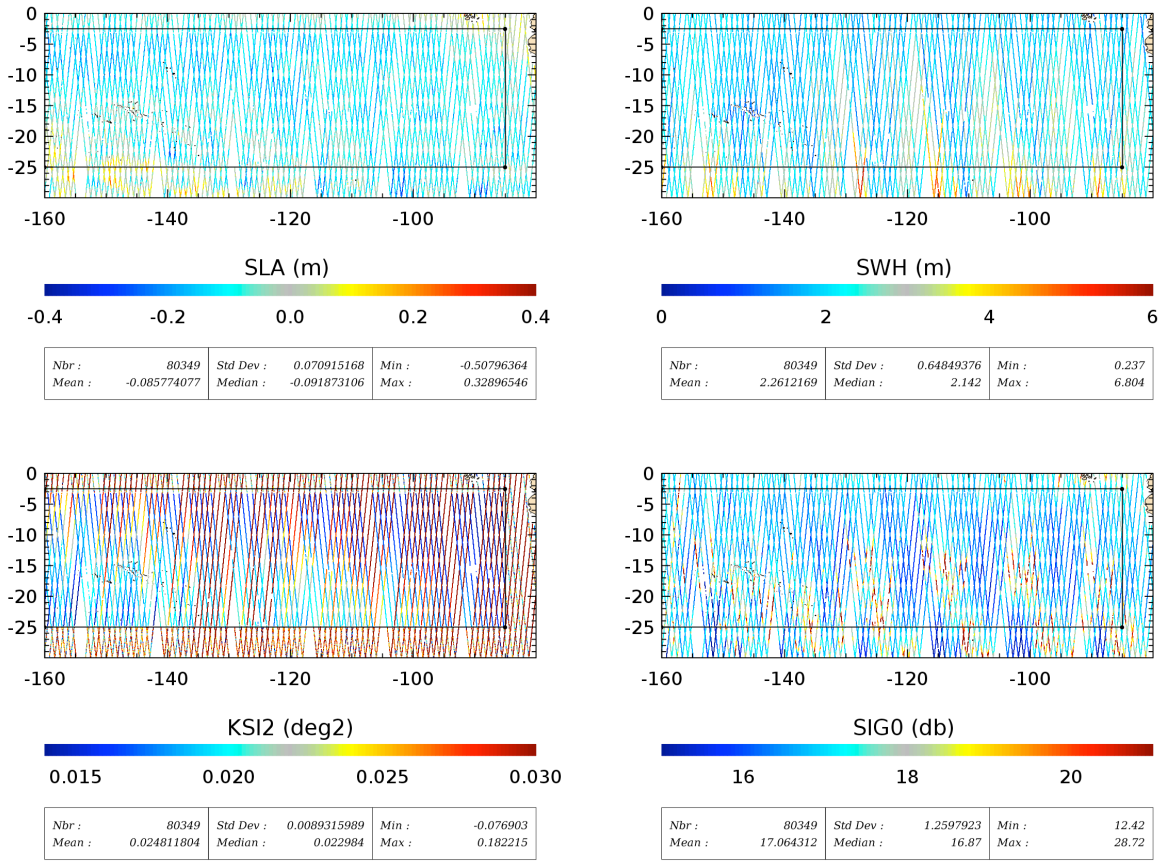

Figure 3.16: Along track SLA (upper left), SWH (upper right), mispointing angles (lower left) and Sigma0 (lower right) data at 1 Hz in LRM mode and SAR mode during subcycle 30. The contour line of the SAR mode area is drawn.

3.4.2. Assessment of the LRM/SAR data continuity

The mean of the SLA, SWH, Sigma-0 and mispointing angle is plotted with respect to latitude in Figure 3.17. Each parameter is averaged per band of latitude of approximately 0.07° and for longitudes from 160° to 85° west (corresponding to the length of the SAR-mode Pacific ocean area). One subcycle of data are integrated and examined.

In these plots, we can see a very good agreement in SLA, SWH and sigma0 coefficient between LRM and RDSAR data at the continuity [RD 3] that is better than the agreement between RDSAR and SAR data over the equatorial Pacific SAR mode area. However there is a very good similarity between RDSAR and SAR data.

On the other hand, the RDSAR mispointing angle and the mispointing angle obtained from star tracker are in quite good agreement, with however the existence of a slightly different trend for which no clear conclusion could be drawn due to the non availability of larger SAR mode areas. In addition, those data are underestimated of 0.06° compared to the LRM estimate that makes the derived along- and across-track mispointing angles method improvable.

This LRM/RDSAR bias may correspond to the error found of estimation of the mispointing angle with respect to simulated mispointing values due to noisier RDSAR waveforms. On-going investigations aim at computing an appropriate LUT to correct the CPP RDSAR data and so resolving this no significant discrepancy.

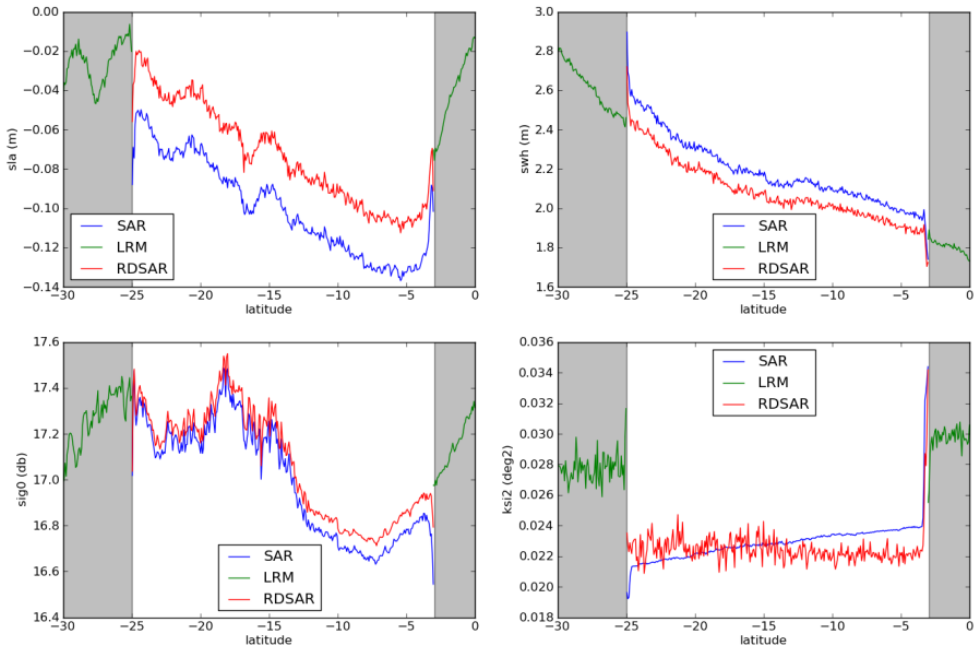

Figure 3.17: Mean of SLA (upper left), SWH (upper right), Sigma0 (lower left) and mispointing angles (lower right) by band of latitude for LRM and RDSAR/SAR of CryoSat-2 - subcycle 30 - pass 82. The dashed zone corresponds to the LRM mode area.

4. Conclusion

The assessment between RDSAR and SAR data has been performed in open ocean in the equatorial Pacific SAR mode region. Results show in general a very good agreement between the two processing, with no significant bias in SLA and SWH. Additionally the SLA/SWH SAR data are more precise than the 1Hz noise obtained with RDSAR values as expected.

As low as they are, the discrepancies in SLA may be explained by the lack of SSB corrections in the RDSAR and SAR dedicated processing, but also by the use of no optimized look-up table correction. Upcoming investigation will focus on the computation of LUT correction for SAR mode (and RDSAR) by taking into account the speckle noise effect, and see whether it will contribute to bring the promising range SAR but also SWH SAR estimates even closer to RDSAR measurements.

After major update of the CPP chain (implemented in version 13), the SAR Sigma0 is now considered for retrieval. First analyses of this parameter have shown very good, promising and unprecedented results. Upcoming feedback from the science users of CryoSat-2 CPP products (that are currently distributed) will contribute to provide other analyses (like wind speed studies) on the quality of the data that will permit to consolidate the CNES implementation of SAR mode processing. Since SAR Sigma0 is now available, a SSB correction, which mainly depends on the SWH and wind speed, may be envisaged to be estimated.

These results obtained over the Pacific demonstrate that the CPP SAR dedicated processing is well suited to derive very accurate and precise SAR altimeter measurements. It also confirm that the Cryosat-2 SAR data and the coming Sentinel-3 data will improve the along track resolution and push for the first time the spatial limit of altimetry down to 30 to 50 km scales, at least in the along track direction.

5. References

[Amarouche et al., 2004]: L. Amarouche, P. Thibaut, O.Z. Zanife, J.-P. Dumont, P. Vincent and N. Steunou, "*Improving the Jason-1 ground retracking to better account for attitude effects*", marine Geodesy, Vol. 27, pp.171-197, 2004.

[Boy et al., 2012]: F. Boy, T. Moreau, J-D. Desjonquères, S. Labroue, N. Picot, J-C. Poisson and P. Thibaut, *"Cryosat Processing Prototype, LRM and SAR Processing"*, presented at the 2012 Ocean Surface Topography Science Team Meeting. Available online: http://www.aviso.oceanobs.com/fileadmin/documents/OSTST/2012/oral/02_friday_28/02_instr_processing_II/02_IP2_Boy.pdf

[Labroue et al., 2013]: S. Labroue, T. Moreau, J-C. Poisson, F. Boy, N. Picot and T. Parrinello, *"Quality Assessment of CryoSat-2 Data Over Ocean in LRM&SAR Modes"*, presented at the 2013 CryoSat third user workshop Meeting.